Charm hadronic decays and quantum correlations at CLEO-c[*]

R. A. Briere[1)]

Department of Physics, Carnegie Mellon University, Pittsburgh, PA 15213, USA

Abstract Several recent CLEO-c results on hadronic decays of charm mesons are reviewed. Topics include measurements of precision branching fractions for exclusive modes, investigations of inclusive rates, and analyses of Dalitz plots. In addition, the quantum correlations of the $D\bar{D}$ pairs produced at the $\psi(3770)$ are exploited to measure phase information that is of current interest for both D and B physics.

Key words charm mesons, hadronic decays, quantum correlations, CKM matrix

PACS 13.25.Ft, 14.40.Lb, 12.15.Hh

1 Introduction

Over the past five years, CLEO-c results have had a large impact on charm physics; we here concentrate on recent hadronic decay results. We first feature significant improvements in the knowledge of D_s meson decay branching ratios. The next set of results involve detailed studies of both D and D_s Dalitz-plot structure.

While the above topics benefit greatly from working near the charm production threshold, the remaining analyses discussed here, related to quantum correlations and coherence, are unique to this energy region. Quantum correlations between the $D\bar{D}$ pairs produced at the $\psi(3770)$ allow an extraction of the strong $K\pi$ scattering phase, which is of interest for D mixing studies. We are also able to extract "coherence factors" in several $D^0 \to K2\pi, K3\pi$ decays; these factors are critical inputs which improve the precision of extractions of the CKM angle γ from B factory data.

Finally, some brief comments on future prospects for hadronic D physics are presented. Since this exposition is of limited length, the interested reader may wish to consult the references for further details.

2 Data samples and techniques

The results presented here are all obtained by CLEO-c. D^+ and D^0 studies use up to 818 pb^{-1} of data taken with e^+e^- collisions near 3770 MeV. The processes $e^+e^- \to \psi(3770) \to (D^+D^-, D^0\bar{D}^0)$, proceed with cross sections of (2.9, 3.7) nb, respectively [1]. Resonance production is accompanied by other reactions, including light-quark pair (uds) continuum, radiative return to the $J\psi$ and $\psi(2S)$, and tau pairs. For D_s studies, we use up to 586 pb^{-1} at 4170 MeV, taking advantage of the channel $e^+e^- \to D_s^{*+}D_s^- +$c.c., with a cross-section of about 0.9 nb [2]. Recall that $D_s^{*\pm} \to D_s^{\pm}\gamma$ occurs 94% of the time, the remainder being $D_s^{\pm}\pi^0$. In addition to the other processes mention above, there is now also about 9 nb of non-strange charm pairs (DD, DD^*, D^*D^*), along with a tiny amount of $D_s^+D_s^-$ [2]. At both energies, it is advantageous that the charm meson pairs of interest are always produced alone, since there is insufficient energy for even one additional pion. We therefore benefit from well-constrained kinematics. Analyses using only part of the available integrated luminosity will be noted below.

Apart from radiative tails, the energy and the magnitude of the momentum of each $D_{(s)}$ are calculable from the well-known machine beam energy. Many analyses also make use of $D_{(s)}$ "tags": a tag is simply a fully-reconstructed $D_{(s)}$ meson. By using tagged events, we largely eliminate non-charm backgrounds and further constrain the other $D_{(s)}$. In particular, in addition to the magnitude of momentum, we now

know the direction of the mesons.

Tags can also be used to constrain the quantum numbers of the mesons. For the phase and coherence factor analyses, it is critical that tags come in several distinct types, as discussed below.

3   Hadronic decay branching ratios

Only a few years ago, knowledge of D_s decays was rather poor. There was an overall 25% systematic error on the branching fraction scale for D_s decays. Modes were referenced to $D_s \to \phi\pi$, which was itself measured with complex techniques of limited precision. There were also not nearly as many modes explored, compared to the non-strange D^0 and D^+ mesons, with particularly limited and imprecise knowledge of inclusive rates.

Major improvements have come out of CLEO-c. Most notably, we present a precise $D_s \to K^+K^-\pi^+$ absolute branching fraction and corresponding Dalitz analysis to use as a reference. Other modes are also improved, or observed for the first time. Combined with a huge leap forward in our knowledge of inclusive rates, this data can greatly improve Monte-Carlo simulations. This is of interest for several flavor-physics experiments, including LHC-b, BESIII, and the B factories.

3.1   Exclusive D_s branching ratios

Invariant-mass peaks for eight exclusive D_s decays, from 298 pb $^{-1}$ of data, are shown in Fig. 1 [3]. Branching ratios are extracted from a global fit to all single-tag (one D_s reconstructed, as in the figure) and double-tag (both D_s decays reconstructed) rates. Simple algebra shows that this tagging technique gives absolute branching ratio results which are independent of the number of $D_s^*D_s$ pairs produced, among other benefits [3]. Requirements are placed on the mass of the system recoiling from the D_s tag, which is a function of the tag momentum; there is a narrow peak from primary D_s and a wider distribution from D_s that come from D_s^* decays. We do not require the transition γ or π^0 from the D_s^* decay. Systematic errors are generally well-studied with data, while efficiencies come from Monte-Carlo simulations.

Our main result is: $\mathcal{B}(D_s^+ \to K^+K^-\pi^+) = (5.50 \pm 0.23\pm0.16)\%$; we also report on the other seven modes shown Fig. 1. More CLEO-c data is available to update these statistics-limited results. The $\phi\pi^+$ submode of $K^+K^-\pi^+$, typically used for normalization, is discussed further in our paper. It should be noted that $\phi\pi^+$ rates obtained with a KK mass cut can be complicated to interpret due to experimental resolution, non-resonant backgrounds, and nearby Dalitz plot features, such as the $f_0(980)\pi^+$.
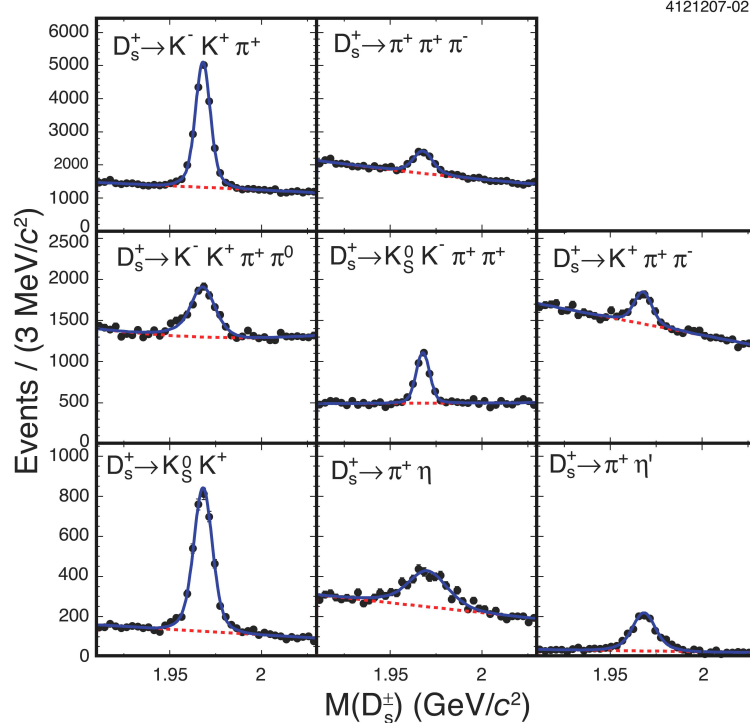
Fig. 1.   Invariant-mass peaks for the eight D_s decay modes studied. The $K^+K^-\pi^+$ channel contains the $\phi\pi^+$ submode, the historical normalization mode for the D_s. The $K^-K^+\pi^+\pi^0$ final state is a first observation.
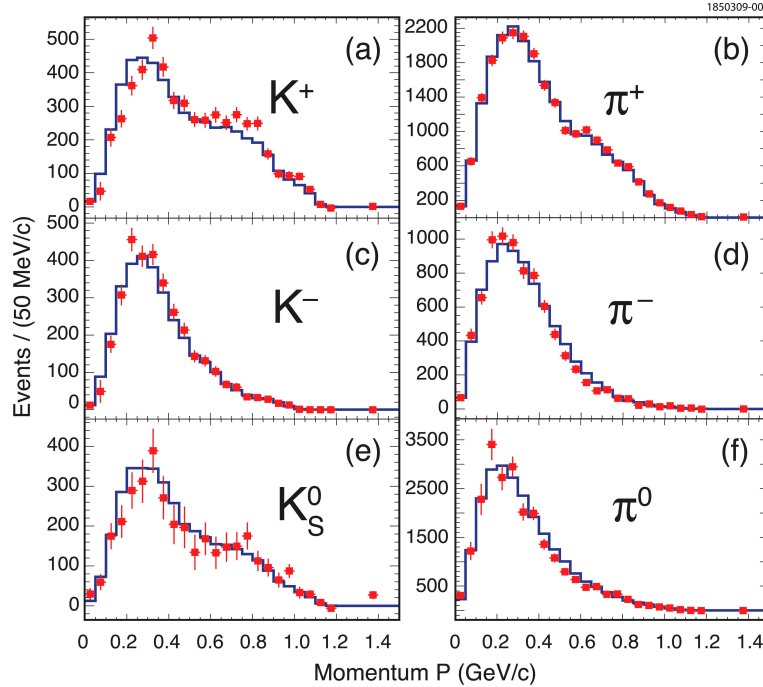
Fig. 2.   Efficiency-corrected and background-subtracted kaon and pion spectra from inclusive D_s^+ decays.

3.2 Inclusive D_s branching ratios

Inclusive branching ratios are also easily studied with fully-reconstructed hadronic tags from our $D_s^{*+}D_s^-$ pairs. Prior to CLEO-c, there were only three (single-particle) inclusive hadronic D_s rates listed, all for kaons, the most precise having a 70% relative error! CLEO-c measured twenty-one rates in total, with much-improved precision.

We use the three best tag modes, $D_s^- \rightarrow \phi\pi^+, K^{*0}K^+, K_S K^+$, the first two being subsets of $K^+K^-\pi^+$. The γ from $D_s^* \rightarrow D_s\gamma$ is required, and cuts are applied to the masses recoiling against the D_s tag and the $D_s\gamma$ system. We find about 18600 tags, with mass sidebands available to correct for backgrounds. Fig. 2 shows inclusive one-particle spectra obtained [4]. Integrated rates to $\eta X, \eta'X, \phi X, \omega X$ are also determined, while a limit is placed on the $f_0(980)X$. We even present a $K_L X$ rate, using tagging and the missing-mass peak obtained when all other particles are found.

Additionally, nine of the ten possible $K\bar{K}X$ rates are reported ($K_L K_L X$ is not feasible). All have significant yields, except the like-sign $K^\pm K^\pm X$ modes. The motivation here is to attempt to shed light on the Feynman diagram topology of the decays. In particular, we obtain lower limits on the contribution of $c\bar{s} \rightarrow W^+ \rightarrow$ hadrons annihilation diagrams. We find a conservative lower bound of $\mathcal{B}(\text{other annihilation}) > 9.5\%$ at 90% C.L., where "other" means that the leptonic annihilation modes $D_s \rightarrow \ell\nu$ are excluded.

3.3 Exclusive D_s decays with an ω

The inclusive rate $\mathcal{B}(D_s \rightarrow \omega X) = (6.1\pm1.4\pm0.3)\%$ found in the previous analysis was intriguingly large, motivating us to investigate exclusive modes with an ω [5]. We find significant yields for $\pi^+\omega, \pi^+\pi^0\omega$, and $\pi^+\pi^+\pi^-\omega$, which already add to $(4.6 \pm 0.9)\%$. Limits are placed on five other modes: $\pi^+\eta\omega, K^+\omega$, $K^+\pi^0\omega, K^+\pi^+\pi^0\omega, K^+\eta\omega$.

4 D^+ and D_S^+ Dalitz plots

We first given an overview of common issues for the three following analyses. We do not use tagging here; although this results in somewhat larger backgrounds, the efficiency is much higher. High statistics are important for observing small features and one can handle the background systematic errors well enough. All fits are based on an "isobar model", which consists of a sum of interfering Breit-Wigners, with correct angular factors. There are many other subtleties and technicalities in the fits; see the references for further details. Some of the more critical of these features include the use of detailed $K\pi$ S-wave treatments, rather than a simple Breit-Wigner resonances, and inclusion of the Flatte formalism for $f_0(980) \rightarrow KK$, which is needed near threshold [6]. We also note that two of the three analyses presented here are "golden modes", used for normalization of other D_s^+ and D^+ decays. High-quality Dalitz fit results

can be used to improve Monte-Carlo models, thus ensuring that other users will get correct efficiencies in order to properly use the integrated branching ratios for normalization. For this aspect, we note that such modeling requires only a good two-dimensional fit of the data, and is not so dependent on subtleties that may be important for physics interpretations.

4.1 $D_s^+ \to K^+ K^- \pi^+$

Our $D_s^+ \to K^+ K^- \pi^+$ uses a sample of more than 12000 signal events with 85% purity [7]. This mode contains the $\phi \pi^+$ final state, the traditional normalization mode for D_s decays. Our data is displayed in Fig. 3.

The resonant submodes considered include $\phi(1020)\pi^+$, $K^*(892)^0 K^+$, $f(980)^0 \pi^+$, $K_0^*(1430)^0 K^+$, $f(1370)^0 \pi^+$, and $f(1710)^0 \pi^+$. All modes except $f(1370)^0 \pi^+$ were used in an analysis of 701 ± 36 events by E687 [8]. For our dataset, adding this mode decreases the χ^2 by 100, to a value of 178 for 117 degrees of freedom. Adding a κ, an S-wave $K\pi$ resonance,

only reduces the χ^2 by five units while adding four degrees of freedom, and is therefore not favored by our data. Fit projections are shown in Fig. 4.
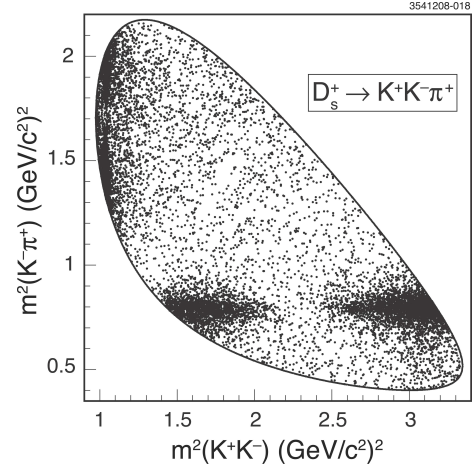
Fig. 3.   Dalitz plot for the $D_s^+ \to K^+ K^- \pi^+$ mode, showing prominent f_0, ϕ bands to the left and K^* band at the bottom.
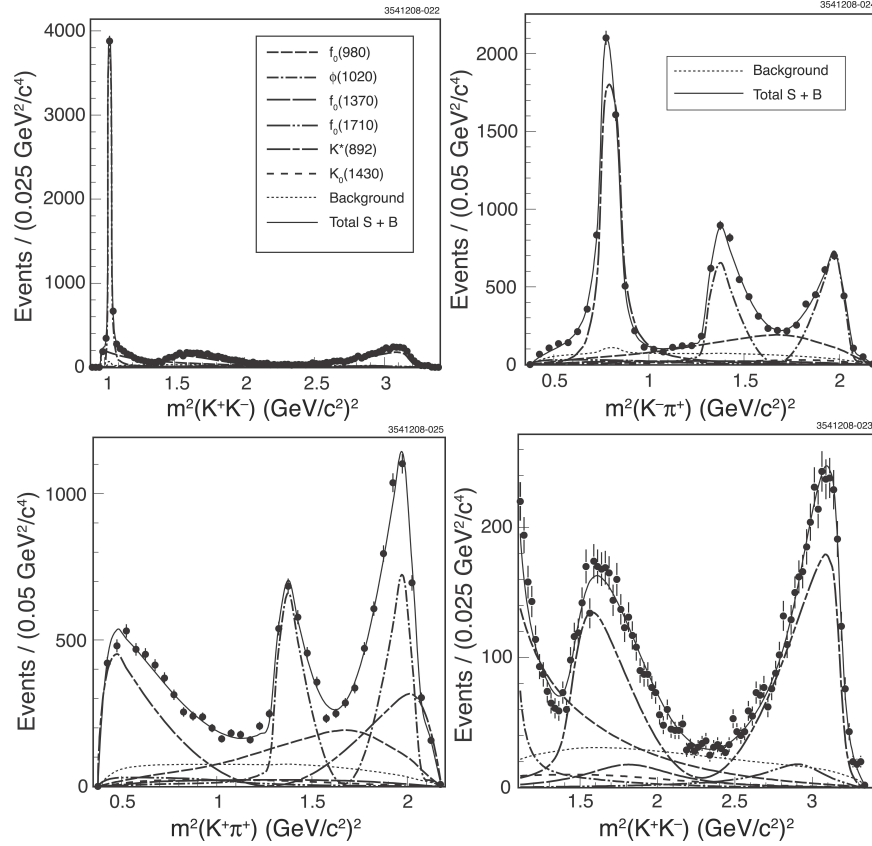
Fig. 4.   Fit projections for the $D_s^+ \to K^+ K^- \pi^+$ mode. Shown are the $K^+ K^-$ mass, the $K^- \pi^+$ mass, the $K^+ \pi^+$ mass, and more detailed look at the KK mass above the ϕ region.

1630708-023
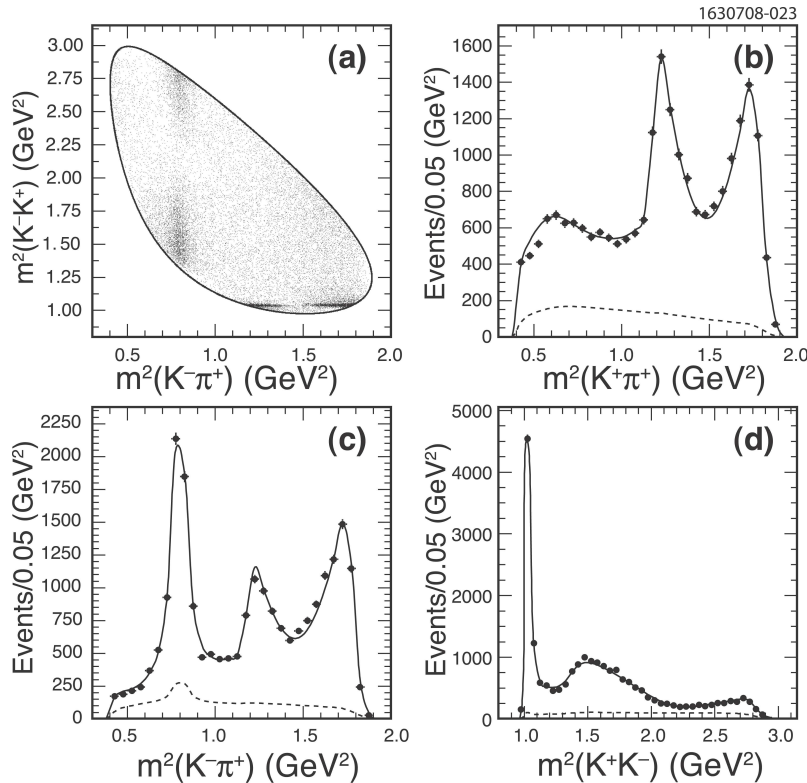
Fig. 5. The $D^+ \to K^+K^-\pi^+$ Dalitz plot, with projections of the fits vs. $K^+\pi^+$ mass, $K^-\pi^+$ mass, and the K^+K^- mass. The ϕ is visibly less dominant (due to Cabibbo-suppression) than for the same final state obtained from D_s decays, as previously presented.

4.2 $D^+ \to K^+K^-\pi^+$

We next discuss $D^+ \to K^+K^-\pi^+$, which is studied with a sample of 19500 signal events at 84% purity [9]. The best fit contains $\phi(1020)\pi^+$, $K^*(892)^0K^+$, $K_0^*(1430)^0K^+$, $a_0(1450)^0\pi^+$, $K_2^*(1430)^0K^+$, $\phi(1680)^0\pi^+$, and κK^+. Using these modes yields a χ^2 of 895 for 708 degrees of freedom. However, replacing the κK^+ final state with a non-resonant amplitude gives a χ^2 of 898 for 708 degrees. Again, as with the previous mode, evidence for the κ is not significant. Fig. 5 displays our data as well as fit projections.

This mode is also used to search for CP violation. Unlike the Cabibbo-favored or doubly-Cabibbo-suppressed decays, this singly-Cabibbo-suppressed mode is sensitive to new physics in penguin diagrams. We find a integrated rate asymmetry of $(-0.03 \pm 0.84 \pm 0.29)\%$; results are also quoted for fit-fraction asymmetries in each resonant sub-mode.

4.3 $D^+ \to K^-\pi^+\pi^+$

The final mode presented here is $D^+ \to K^-\pi^+\pi^+$, using more than 139,000 events with 99% purity [10]. This is the key normalization mode for D^+ decays, and an interesting place to study $K^-\pi^+$ behavior.

We start with the same model originally used by E791 [11]: $K^*(892)^0\pi+$, $K_0^*(1410)^0\pi+$, $K_2^*(1430)^0\pi+$, $K^*(1680)^0\pi+$, $\kappa\pi^+$, plus a non-resonant term. Our fit has a χ^2/dof of 531/391; and the $\kappa\pi^+$ term has the largest fit fraction. However, we find that the fit can be significantly improved, and the apparent evidence for the κ is needs to be more carefully considered.

First, adding an $I = 2$ $\pi\pi$ S-wave improves the χ^2/dof to 416/385, a rather striking improvement. Further improvement is achieved by replacing the both the $\kappa\pi^+$ and non-resonant terms with a "binned S-wave" description of the $K\pi$ amplitude, as later done by E791 [12]; this gives a χ^2/dof to 359/347. By binned S-wave, we mean that the amplitude and phase of the $K\pi$ S-wave are freely floating in each of 26 different mass bins, spanning $0.4 < m_{K\pi}^2 < 3.0$ GeV$^2/c^2$. While this adds a significant number of degrees of freedom, the χ^2 reduction is nonetheless significant. In Fig. 6, we show the binned fit results We find that both the amplitude and phase of the $K\pi$ S-wave are rather slowly varying. While this behavior can be approximated by a constant non-resonant amplitude in combination with a very broad resonance (κ), we obtain the best fit with this quasi-model-independent binned treatment.
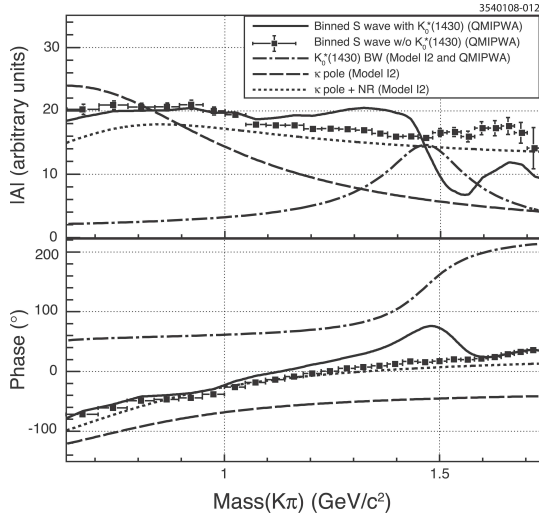
Fig. 6. The S-wave $K^-\pi^+$ amplitude (top: magnitude, bottom: phase) in $D^+ \to K^-\pi^+\pi^+$ decays. Our main fit is shown by the large square points with error bars. Ref. [10] contains further details.

5   Quantum correlations and phases

The decay of the $J^{PC} = 1^{--}$ $\psi(3770)$ results in a correlated $D^0\bar{D}^0$ system. The final state is pure P-wave, and hence the quantum numbers of the mesons are completely entangled with each other. Not only can correlated behavior be observed in the subsequent D decays, but it can also employed to study quantities related to $D^0-\bar{D}^0$ mixing. Most interesting is sensitivity to the strong-scattering phase of the $K^-\pi^+$ system, $\delta_{K\pi}$ [13].

Decaying mesons may have definite flavor (D^0 vs. $\bar{D}^0$), be superimposed as a CP-eigenstate, or even be an approximate flavor tag with "DCSD" contamination.

5.1   Global analysis for $\delta_{K\pi}$

CLEO-c has performed a detailed analysis of quantum correlations using an integrated luminosity of 281 pb^{-1} [14, 15]. The analysis uses eight single-tag modes, twenty-four fully-reconstructed double-tags combinations, fourteen varieties of inclusive electrons vs. single tags, and five modes with $K_L\pi^0$ vs. a single tag. Fig. 7 shows some of the single-tag mass peaks.

The clearest sign of quantum correlations is in the enhancement of a $CP = -1$ D^0 decay with a $CP = +1$ $\bar{D}^0$ decay (or vice-versa) and the related absence of two $CP = +1$ or two $CP = -1$ decays. Theoretical predictions and results are compared in Fig. 8, clearly confirming the expected behavior.
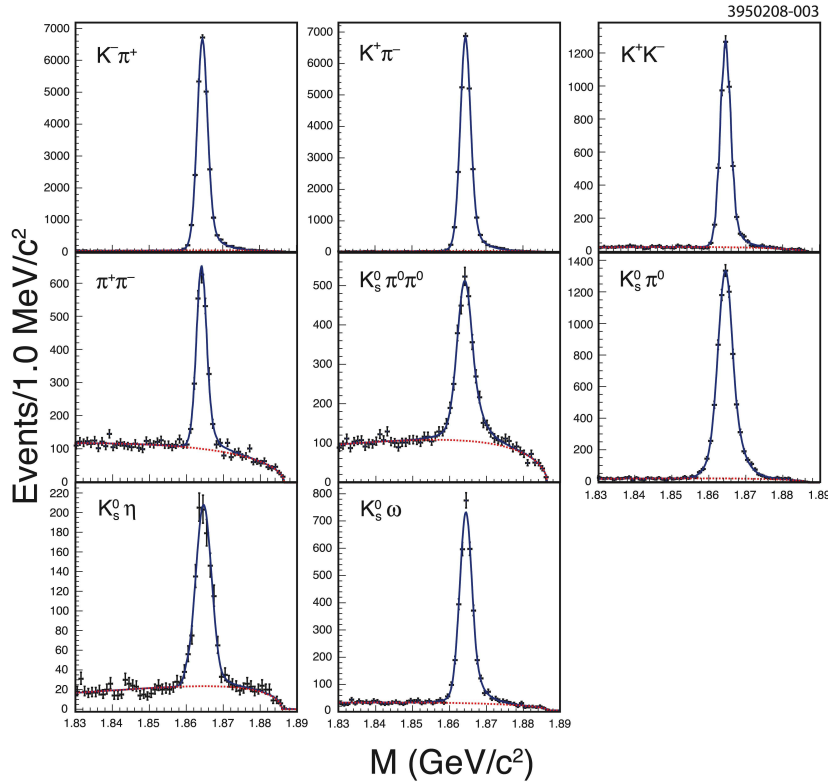
Fig. 7. Some of the tag modes used in the quantum correlation analysis. The first two are approximate flavor-tags (with DCSD admixtures), the next three are $CP = +1$ eigenstates, and the last three are $CP = -1$.
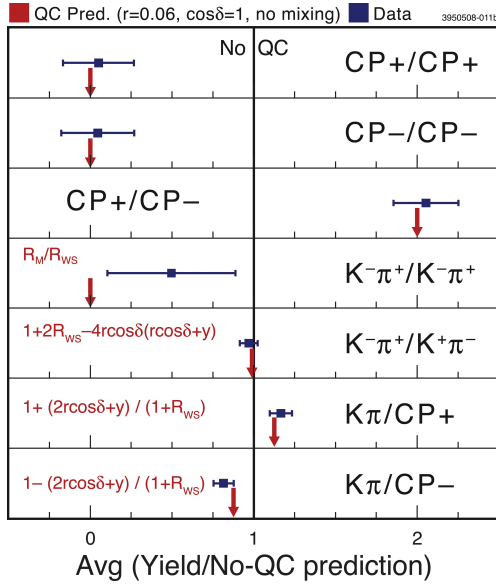
Fig. 8. Quantum correlation effects are illustrated via comparisons of the CLEO-c measurements (blue) and predictions (red). All values are normalized to the naive predictions in the absence of correlation effects; excellent agreement is evident.

Smaller effects are related to several interesting quantities. First, there are the $D^0 - \bar{D}^0$ mixing parameters x, y, where $x = \Delta M/\Gamma$ and $y = \Delta\Gamma/2\Gamma$. Second, there are flavor "contaminations", due to doubly-Cabibbo-suppressed decays (DCSD) interacting with Cabibbo-allowed (CA) amplitudes, which are parameterized by the amplitude ratios $r = \mathcal{A}_{CA}/\mathcal{A}_{DCSD}$. Detailed but straightforward calculations (see [13]) reveal sensitivity to the strong $K\pi$ final-state-interaction (FSI) phase shift, $\delta_{K\pi}$. This phase is necessary to extract x, y from D-mixing studies performed with the $K^\mp\pi^\pm$ mode.

With CLEO-c statistics, we are not very sensitive to mixing, and thus use external mixing constraints on x, y to improve our fit. Likelihood contours resulting from the fits are displayed in Fig. 9. We find that $\delta = (22^{+11}_{-12}{}^{+9}_{-11})^\circ$.

Almost three times more data in the full CLEO-c sample, combined with a variety of analysis improvements (chiefly additional mode combinations), should eventually reduce the statistical errors by a factor of two.
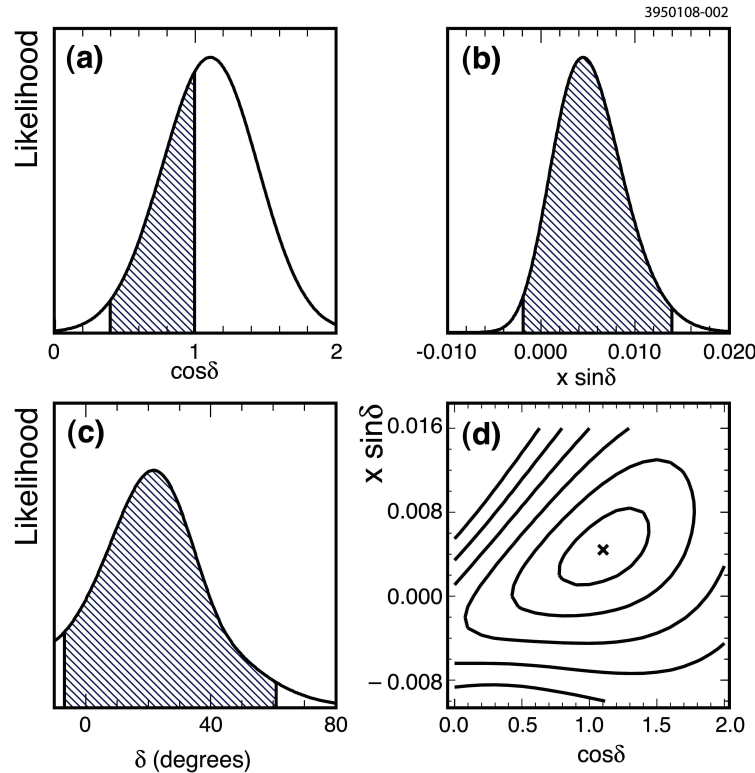
Fig. 9. Likelihood contours from the "extended" fit which uses external inputs in addition to CLEO-c data. See in particular the left colum, with $\cos\delta$ and δ. Shading indicated 90% of the physical regions.

5.2 Coherence factors for three $Kn\pi$ modes

Interference effects in two-body modes in general depend on a phase, such as $\delta_{K\pi}$ discussed above.

For multi-body modes, these quantities now vary with location in phase space. A toy model will suffice to give a sense of the relevant behavior. For two complex amplitudes $A, \bar{A}$, with relative phase ϕ,

$|A+\bar{A}|^2 = |A|^2 + |\bar{A}|^2 + 2|A\bar{A}|\cos\phi$. If the amplitudes for D^0 and $\bar{D}^0$ decay were identical, then we would have $R = 1$ and $\delta = 0$. For two-body modes, such as $K^-\pi^+$, $R = 1$, and only a relative phase δ is unknown. But when $A, \bar{A}$ vary in size and relative phase across a Dalitz plot, integrating the data replaces the $2\cos\phi$ in the cross term with $2R\cos\delta$. These "coherence factors", R, δ, can only be measured with the use of CP tags, which are unique to charm threshold data. Opposite CP tags, we have the decay of the coherent superpositions $D_{1,2} = (D^0 \pm \bar{D}^0)/\sqrt{2}$, and are hence able to observe the interference, and hence the relative phase, of the D^0 and $\bar{D}^0$ decay amplitudes.

The values of R, δ for various D^0 modes are of interest for determinations of the CKM angle γ from B decays, using modes where the B decay includes a $D^0, \bar{D}^0$ in the final state. Fig. 10 shows the results of our analysis for the $K^-\pi^+\pi^0$ and $K^-\pi^-\pi^+\pi^+$ modes [16]. The first mode is very coherent, giving larger interference and good sensitivity to γ. While the sec-

ond mode seems less useful due to the lack of large coherence, it turns out to be useful to also have such modes as well. In particular, this allows one to constrain properties of the B meson decays more cleanly, independent of D meson physics.

The decay $D^0 \to K_S\pi^+\pi^-$ also may be used with B decays to extract γ; the analysis performed by CLEO-c differs from that discussed above in two ways. First, phase space is divided into eight different bins to enhance sensitivity, with the coherence parameters measured separately in each bin. Second, the parameters R, δ are replaced by two equivalent variables c_i, s_i. These quantities, $c_i = \langle R\cos\delta\rangle_i$ and $s_i = \langle R\sin\delta\rangle_i$, are averaged across each bin (labeled by i). In Figs. 11 and 12, we show the difference between the $K_S\pi^+\pi^+$ decays from the different CP-eigenstates which we separate opposite our CP-eigenstate tags. Note the marked differences in these two sets of plots. We also use $K_L\pi^+\pi^-$ decays in this analysis.
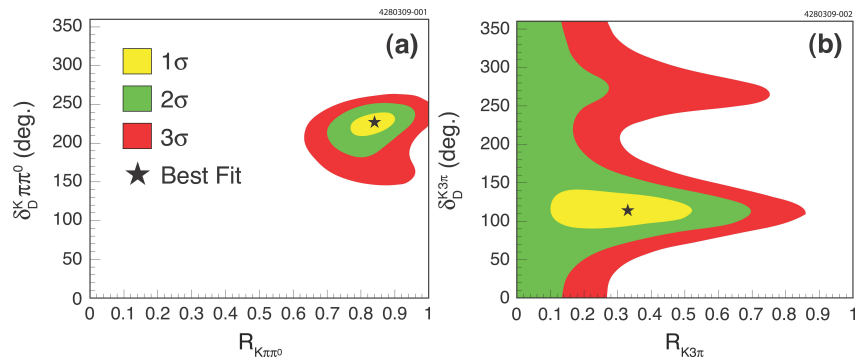
Fig. 10. Left: coherence factor results shown as likelihood contours for the $K^-\pi^+\pi^0$ mode. D^0 and D^0 bar decays are similar in this case, and the results are not so far from $R = 1, \delta = 180°$. Right: Coherence factor results shown as likelihood contours for the $K^-3\pi^-\pi^+\pi^+$ mode. There is significantly less coherence in this mode.
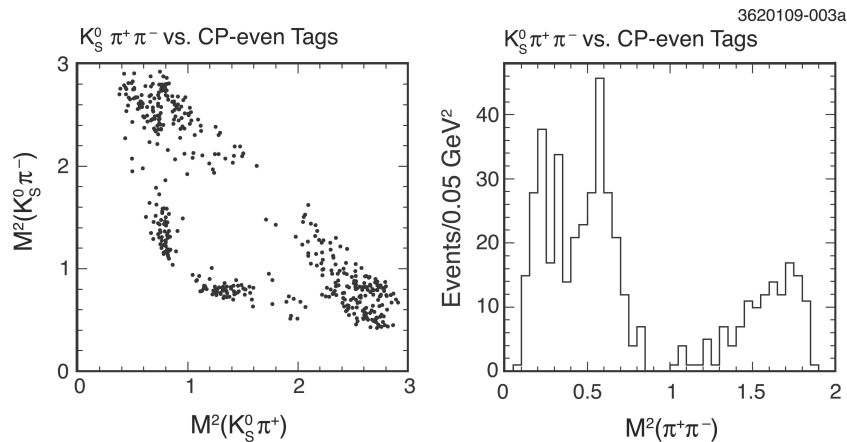
Fig. 11. Dalitz plot and $\pi^+\pi^-$ mass-squared projection for $D^0 \to K_S\pi^+\pi^-$ decays reconstructed opposite $CP+$ tags. Compare to the $CP-$ tags below.
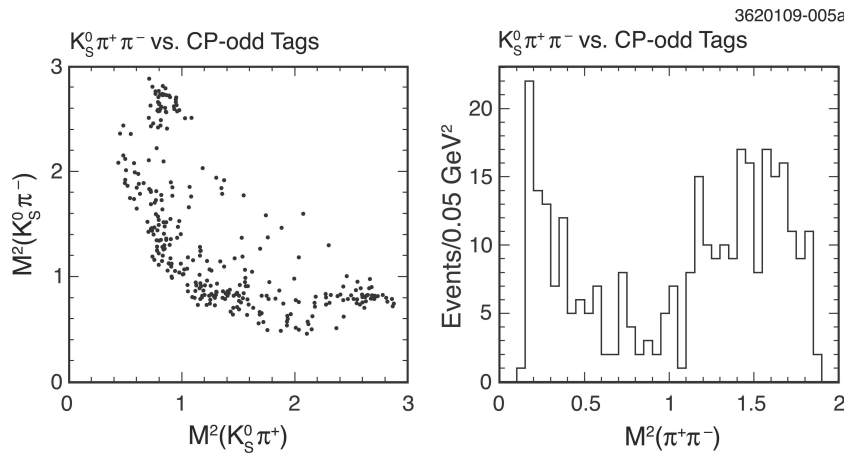
Fig. 12.　Dalitz plot and $\pi^+\pi^-$ mass-squared projection for $D^0 \to K_S\pi^+\pi^-$ decays reconstructed opposite $CP-$ tags.
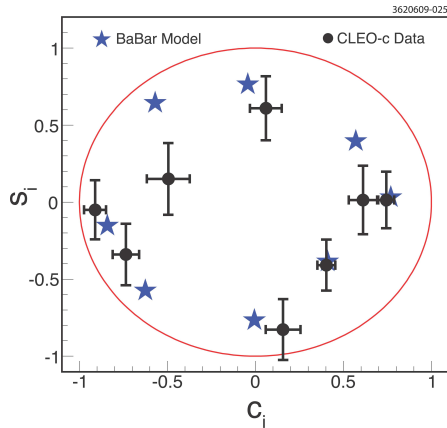
Fig. 13.　Binned coherence factors for the $D^0 \to K_S\pi^+\pi^-$. CLEO data (points with error bars) are compared to a prior BaBar model (stars).

Figure 13 compares the extracted CLEO-c results [17] to a model. While this previous model was quite good, the advantage of having a direct measurement is that it allows a clean determination of the systematic error contribution from the structure of the $K_S\pi^+\pi^-$ mode. Studies predict the CLEO-c results

reduce this uncertainty from about $7°$ to less than $2°$, which is more in line with forthcoming experimental statistical precisions on γ.

6　Conclusion and prospects

CLEO-c's return to charm threshold 20 years after MARKIII has led to a wealth of new results on charm hadronic decays (and other topics). While many analyses are complete, not all of the statistics-limited analyses have yet used the full CLEO-c datasets. Furthermore, in early 2010, BESIII will begin to collect open-charm data, initially at the $\psi(3770)$. Since the BEPCII collider has already supplied luminosities more than four times larger than CESR-c was able to deliver to CLEO-c, precision analyses from charm threshold techniques should continue to appear for many years to come.

References

1　Dobbs S et al (CLEO collaboration). Phys. Rev. D, 2007, **76**: 112001
2　Cronin-Hennessy D et al (CLEO collaboration). Phys. Rev. D, 2009, **80**: 072001
3　Alexander J P et al (CLEO collaboration). Phys. Rev. Lett., 2008, **100**: 161804
4　Dobbs S et al (CLEO collaboration). Phys. Rev. D, 2009, **79**: 112008
5　GE J Y et al (CLEO collaboration). Phys. Rev. D, 2009, **80**: 051102
6　Flatte S M. Phys. Lett. B, 1976, **63**: 224
7　Mitchell R E et al (CLEO collaboration). Phys. Rev. D, 2009, **79**: 072008
8　Frabetti P L et al (E687 collaboration). Phys. Lett. B, 1995, **351**: 591
9　Rubin P et al (CLEO collaboration). Phys. Rev. D, 2008, **78**: 072003
10　Bonvicini B et al (CLEO collaboration). Phys. Rev. D, 2008, **78**: 052001
11　Aitala E M et al (E791 collaboration). Phys. Rev. Lett., 2002, **89**: 121801
12　Aitala E M et al (E791 collaboration). Phys. Rev. D, 2006, **73**: 032004
13　Asner D M, Sun W M. Phys. Rev. D, 2006, **73**: 034024 2008, **77**: 019901
14　Asner D M et al (CLEO collaboration). Phys. Rev. D, 2008, **78**: 012001
15　Rosner J L et al (CLEO collaboration). Phys. Rev. Lett., 2008, **100**: 221801
16　Lowrey N et al (CLEO collaboration). Phys. Rev. D, 2009, **80**: 031105
17　Briere R A et al (CLEO collaboration). Phys. Rev. D, 2009, **80**: 0312002